Catalysis Letters Vol. 100, Nos. 3–4, April 2005 (© 2005)
DOI: 10.1007/s10562-004-3436-7

Fabrication of platinum nanoparticles and nanowires by electron beam lithography (EBL) and nanoimprint lithography (NIL): comparison of ethylene hydrogenation kinetics

A. M. Contreras[a,b,*], J. Grunes[a,b], X. -M. Yan[b], A. Liddle[b], and G. A. Somorjai[a,b]

[a]*Department of Chemistry, University of California, Berkeley, CA 94720, USA*
[b]*Materials and Chemical Sciences Divisions, Lawrence Berkeley National Laboratory, Berkeley, CA 94720, USA*

Received 15 November 2004; accepted 14 December 2004

Electron beam lithography (EBL), size reduction lithography (SRL), and nanoimprint lithography (NIL) have been utilized to produce platinum nanoparticles and nanowires in the 20–60-nm size range on oxide films (SiO_2 and Al_2O_3) deposited onto silicon wafers. A combination of characterization techniques (SEM, AFM, XPS, AES) has been used to determine size, spatial arrangement and cleanliness of these fabricated catalysts. Ethylene hydrogenation reaction studies have been carried out over these fabricated catalysts and have revealed major differences in turnover rates and activation energies of the different nanostructures when clean and when poisoned with carbon monoxide. The oxide-metal interfaces are implicated as important reaction sites that remain active when the metal sites are poisoned by adsorbed carbon monoxide.

KEY WORDS: ethylene hydrogenation; CO poisoning; electron beam lithography; size reduction lithography; nanoimprint lithography; platinum nanoparticles; platinum nanowires.

1. Introduction

Metal single crystals have long been used as model catalysts in combined surface science and catalytic reaction studies. Platinum single crystals of different orientation crystal faces have been used for H_2/D_2 exchange [1–3], CO oxidation [4,5], and hydrocarbon conversion reactions like ethylene hydrogenation [6–16]. They revealed the surface structure sensitivity or insensitivity of different catalytic reactions, the roles of surface defects such as steps and kinks, and additives that are bonding or structure modifiers. Many industrial platinum catalysts are nanoparticles that are dispersed on high surface area porous oxide supports. The resistance of these industrial catalysts to poisoning under industrial conditions has been the focus of much research, and it has been postulated that this may be due to the presence of an oxide-metal interface. Single crystals provide a wealth of information about adsorbate bonding to different crystal faces and catalytic reaction mechanisms, but are unable to successfully model reactivity intrinsic to industrial catalysts that involve the oxide-metal interface or the oxide surface. One direction of research in our laboratory is to bridge this gap between the catalytic chemistry of model single crystals and high surface area platinum nanocluster catalysts used in the chemical technologies. There has been considerable effort to create a model catalytic system with an oxide-metal interface that can be tuned precisely in the nanometer size range. While turnover frequencies are measured under many conditions for various oxide-metal systems, the nature of the catalytically active sites in industrial catalysts is not well understood. With precise control of the fabrication of a catalyst comes the ability to systematically vary different parameters of the metal structure such as size and spacing as well as a choice of the oxide-metal interface of the catalyst. Control of these parameters in the nanoscale regime is difficult to obtain, but lithography lends itself nicely to this task. To this end, we first explored the use of electron beam lithography (EBL) to construct platinum nanoparticle arrays on oxide surfaces as new model platinum catalysts [17,18]. Approximately 10 [9] nanoparticles could be produced using this technique on a 1-cm^2 silicon wafer in about a day. This corresponds to a platinum surface area of about 0.1 cm^2. However, the study of low turnover reactions ($< 10^{-4}$ s^{-1}) requires $\sim$1 cm^2 of platinum surface area for practical detection of reaction products. Because of the sequential nature of electron beam exposure, the production of $\sim$1 cm^2 of exposed platinum surface area would require approximately 10 days to fabricate, which is not practical. While the EBL-fabricated platinum samples could be used to study high turnover reactions (such as ethylene hydrogenation) or the thermal and chemical stability of the platinum nanoparticles, we turned to another technique, photolithography, to fabricate higher surface area nanoarrays of platinum cata-

* To whom correspondence should be addressed.

1011-372X/05/0400–0115/0 © 2005 Springer Science+Business Media, Inc.

lysts. Photolithography techniques have been used successfully in the microelectronic industry for years and have proven successful in creating sub-μm structures with high degree of uniformity and reproducibility [19–21]. Size reduction lithography (SRL), developed in our laboratory, couples photolithography with low-pressure chemical vapor deposition and reactive-ion etching techniques to create structures smaller than the normal diffraction limits of photolithography. When this size-reduction technique is used multiple times, it can drastically increase feature density. SRL has previously demonstrated the ability to produce a silicon mold with nanowire structures of 7-nm diameter [22,23]. It has also been shown, that a silicon mold can be used in nanoimprint lithography (NIL) to reproduce sub-10 nm features by using the mold to imprint its features into a polymer resist and depositing the desired material into the negative of the mold pattern [24–26]. The NIL process is a practical fabrication method, which offers a high-throughput method with low production cost, and a choice of deposition materials and substrates. Here, SRL has been used in conjunction with NIL to fabricate arrays of platinum nanowires. After using photolithography and SRL to produce a silicon mold with nanowire features, the mold was used to imprint its features into a polymer resist. This imprint was followed by platinum deposition through the imprinted features to produce platinum replicas of the original silicon mold on either a SiO_2 or Al_2O_3 surface.

This paper describes the production of platinum nanocatalyst arrays fabricated by EBL and NIL to create nanoparticle and nanowire arrays, respectively. We use these platinum nanoarrays to carry out ethylene hydrogenation with and without the presence of carbon monoxide. Surprisingly large differences in turnover rates and activation energies were found for the different nanocatalysts even for this structure insensitive reaction. The collected experimental data points to the important catalytic role of the oxide-metal interface especially when the platinum sites are poisoned using carbon monoxide.

2. Experimental

2.1. Platinum nanoparticle arrays on alumina and silica: fabrication by EBL and characterization

The EBL fabrication process of platinum nanoparticle arrays has been reported elsewhere [17,18], and the general scheme is shown in figure 1a. Briefly, a thin layer of electron sensitive polymer resist is spincast onto a Si(100) wafer coated with a 15-nm thick film of either alumina (Al_2O_3) or silica (SiO_2). The photoresist used was poly-methyl methacrylate (PMMA) with M_w = 950 k. The resist is exposed to a highly collimated electron beam (Leica Nanowriter) in a computer-generated dot-like pattern across the polymer surface. The electron beam is generated by a field emission source that exposed the polymer with a beam current of 600 pA and an accelerating voltage of 100 kV giving the beam a diameter of approximately 3 nm. Upon exposure to the electron beam, the polymer undergoes bond scission, which renders it more soluble in a developer solution. After developing the pattern, 15 nm of Pt is vacuum deposited onto the exposed underlying oxide substrate by means of electron beam evaporation using a quartz crystal microbalance thickness monitor. Liftoff of the remaining polymer is achieved by ultrasonication in acetone for 5 min, leaving an array of Pt nanoparti-

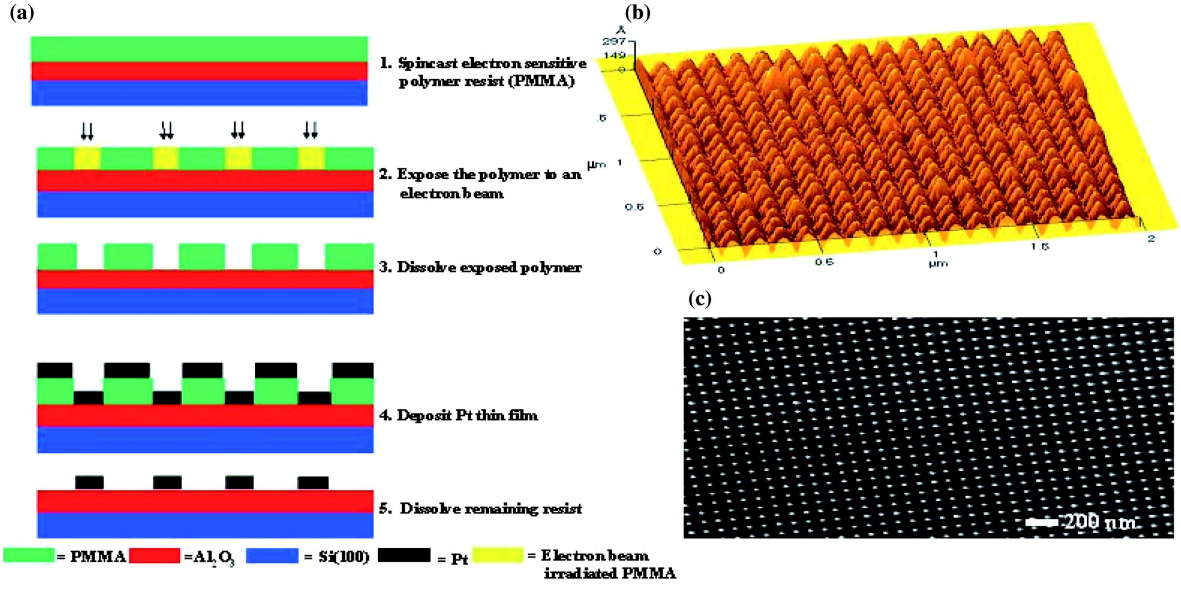

Figure 1. (a) EBL fabrication scheme (b) Atomic force microscopy image of Pt nanoparticle array showing Pt particle height of 15 nm (c) Scanning electron microscopy image of Pt nanoparticle array showing particle diameters of 28 nm and particle spacing of 100 nm.

cles on the surface. Atomic force microscope (AFM) and scanning electron microscope (SEM) images of the platinum arrays on an alumina substrate are shown in figure 1b and c, respectively.

2.2. *Platinum nanowire arrays on alumina and silica: fabrication by NIL and characterization*

The process for using SRL to define a nanowire array on a single-crystalline Si surface has been detailed previously [22,23]. Briefly, the Si mold used for fabrication of Pt nanowire arrays was fabricated by first growing a 50–70 nm thermal SiO_2 layer onto the surface of a Si(100) wafer. Next, a 100-nm polysilicon layer is deposited by low-pressure chemical vapor deposition (LPCVD) at 873 K as a sacrificial layer. A positive photoresist is spincast onto the poly-Si layer and exposed to radiation through a patterned mask. The radiation-exposed polymer is removed with developing solution. This leaves the unexposed, patterned photoresist on top of a polysilicon layer. This pattern is then transferred into the underlying polysilicon layer by reactive-ion etching in a HBr and Cl_2 plasma (LAM TCP 9400). The remaining 20–30 nm of photoresist is then stripped off in oxygen plasma. An SEM image of the polysilicon features is shown in figure 2b. At this point, a low-temperature silicon oxide (LTO) layer is deposited over the defined polysilicon pattern by low-pressure chemical vapor deposition at 723 K. This is a conformal deposition and coats the entire patterned surface. The thickness of the sidewall deposition during this step will define the ultimate feature size. The LTO layer on top of the sacrificial polysilicon feature is anisotropically etched away in CF_4 plasma. The exposed polysilicon feature is then selectively etched away leaving an LTO pattern of nanowires on the thermal oxide underlayer. These wire features are transferred into the thermal oxide layer by anisotropic etching with CF_4 plasma. The thermal oxide pattern is then transferred into the single-crystalline Si wafer by anisotropically etching with HBr and Cl_2 plasma. 20-nm silicon nanowires are routinely produced by this process. This process is pictured schematically in figure 2a. Oxidative trimming techniques are then used to reduce the nanowire width. The wafer is thermally oxidized at 1073 K for 30 min and then dipped into HF for oxide removal, reducing the wire width to 7 nm. The nanowire features on the Si mold used in the preparation of samples for this study had a height of 110 nm, and a width of 7 nm (figure 2c).

This Si nanowire pattern was used as a mold to reproduce its patterns by use of NIL. The NIL fabrication method used to create our catalysts is shown schematically in figure 3a. Previous to using the silicon

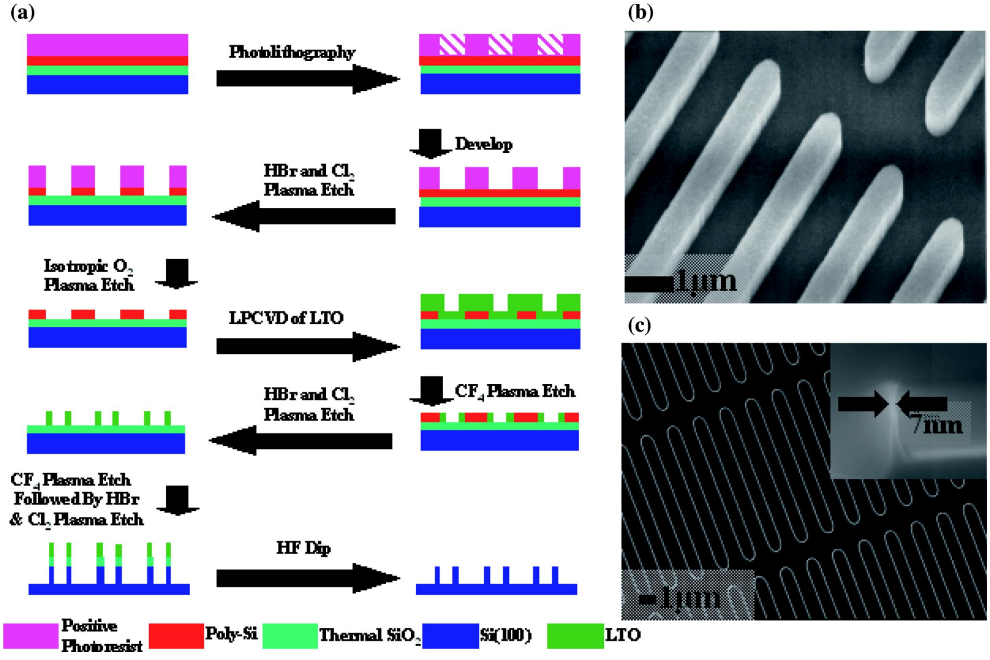

Figure 2. (a) SRL Scheme used for fabrication of Si nanowire mold. A Si(100) wafer is used to grow a thermal oxide (SiO_2). A polysilicon layer is then grown by low-pressure chemical vapor deposition (LPCVD) on top of the thermal oxide. A positive photoresist is spincast onto the poly-Si surface and exposed to radiation through a patterned mask. The pattern is developed and etched into the poly-Si layer with HBr and Cl_2 plasma. A conformal deposition of low temperature oxide (LTO) covers the poly-Si features, and the sidewalls of this deposition define the new feature size. The poly-Si feature is exposed by a CF_4 plasma etch. The poly-Si is then selectively removed by an HBr & Cl_2 plasma etch. The pattern can now be transferred into the Si wafer by etching through the SiO_2 layers with CF_4 plasma followed by HBr & Cl_2 plasma to etch the pattern into the wafer. An HF dip cleans the surface of all SiO_2 and leaves the features made of single crystal silicon. (b) SEM image of polysilicon features on SiO_2 support. Features have a 600-nm width with 1.2 μm spacing. (c) SEM image of final silicon mold with nanowire pattern. Wires are Si(100) as is the support. The inset shows the 7-nm sidewall of the silicon nanowire pattern.

mold for imprinting, the surface is functionalized by physical vapor deposition of a fluoropolymer, which acts as a lubricant. The fluoropolymer used to functionalize the silicon surface is (tridecafluoro-1,1,2,2-tetrahydrooctyl)-1-trichlorosilane or $C_6F_{13}C_2H_4SiCl_3$ (FTS). The FTS solution prepared was 10% by mass in *n*-octane. The FTS solution is physical vapor deposited onto the silicon mold surface at 343 K for 5 min. Contact angle measurements on the silicon mold showed a water contact angle of approximately 100° after deposition of the fluoropolymer. This surface functionalization lowers the surface energy of the mold, so that separation of the mold from the imprinted polymer substrate is more facile. The polymer used for our imprinting was PMMA (M_w = 15 k). The PMMA solution prepared was 4% by mass in chlorobenzene. This solution is spincast at 900 RPM onto a Si(100) wafer coated with either 15 nm of alumina or silica. The sample is then baked at 363 K for 5 min to remove residual solvent. The resultant PMMA films have an average thickness of about 180 nm measured by reflectometry. The PMMA coated substrate and Si mold are placed in contact with each other for imprinting. The mold and substrate are heated to 400 K (PMMA T_g = 378 K) and pressed to 4000 PSI (27.6 MPa) for 5 min. The mold and substrate are then cooled under pressure by flowing N_2 gas over the imprinting apparatus and subsequently separated at room temperature leaving the negative pattern of the Si mold in the PMMA layer. It was found that a better imprint resulted from more rapid cooling with N_2 gas rather than allowing the apparatus to cool slowly. To remove the remaining polymer from the bottom of the imprinted features it is necessary to etch the pattern deeper into the polymer layer. To avoid any broadening from this etching and in an attempt to control the final feature size, 15 nm of SiO_2 is shadow deposited by electron beam evaporation at an optimized 45° angle with respect to the evaporation source. The substrate is then rotated 180° and 15 nm of SiO_2 is again evaporated at a 45° angle with respect to the evaporation source. At this point, the remaining PMMA at the bottom of the

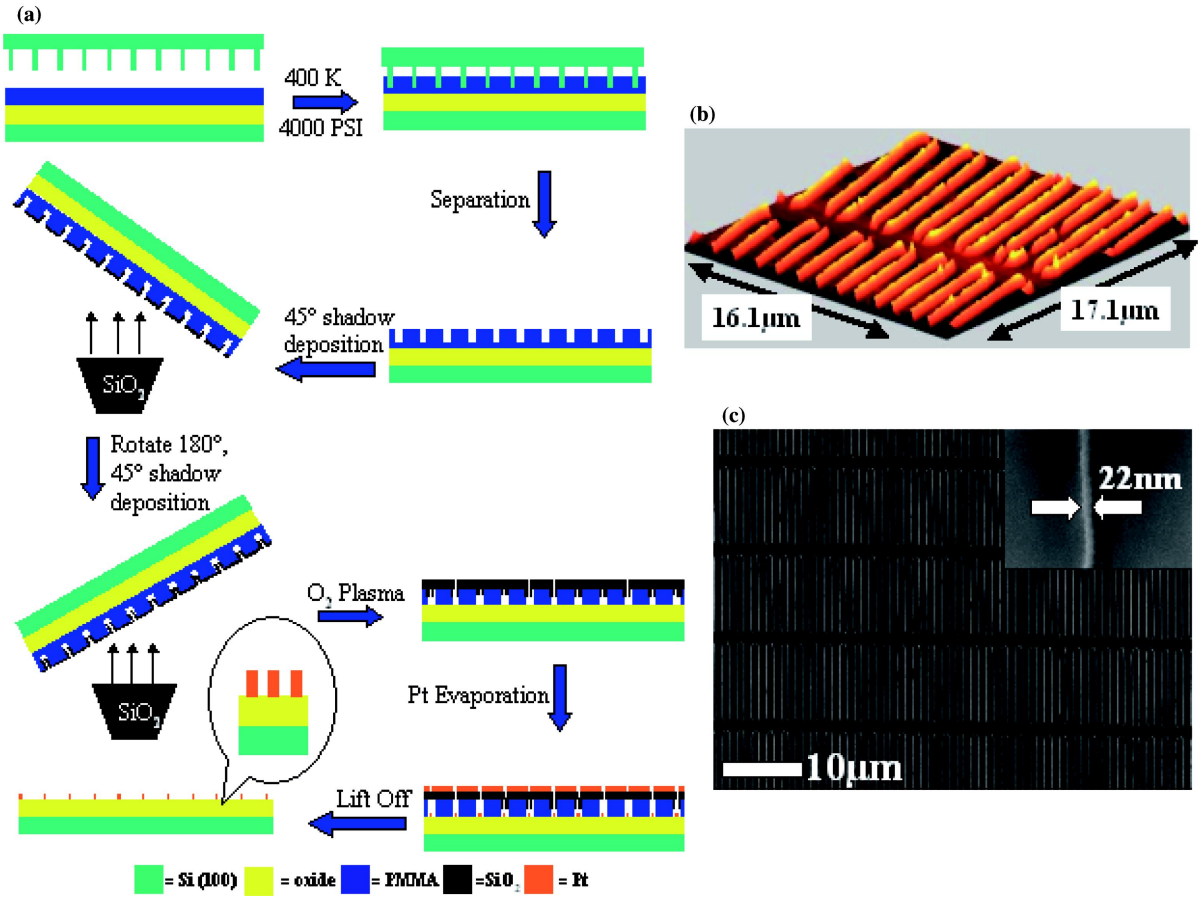

Figure 3. (a) Nanoimprint lithography fabrication scheme. PMMA is spincast onto an oxide-coated wafer and placed in contact with the Si mold. The mold and PMMA-coated wafer are heated to 400 K and pressed to 4000 PSI for 5 min. Fifteen nanometers of SiO_2 is deposited by electron beam evaporation at a 45° angle. The sample is rotated 180° and another 15 nm of SiO_2 is deposited at a 45° angle. The remaining PMMA at the bottom of the imprinted features is removed by an O_2 plasma etch. 15 nm of platinum is deposited onto the exposed oxide surface and remaining PMMA is removed by submersing the sample in acetone and ultrasonicating for 5 min. (b) AFM image of Pt nanowires on alumina support showing 15-nm height of wires. (c) SEM image of Pt nanowires on alumina support. Inset shows 22-nm width of wires.

imprinted features is removed by O_2 reactive-ion etching (LAM TCP 9400) using 10 mTorr O_2 pressure, a flow of 100 sccm with the top and bottom electrodes set at 100 and 25 W, respectively. After etching the residual polymer layer away, 15 nm of Pt is vacuum deposited, by electron beam evaporation with a quartz crystal microbalance thickness monitor. The Pt is deposited through the imprinted pattern and onto the exposed oxide support. The remaining polymer is removed by ultrasonication in acetone for 5 min, leaving a Pt array of nanowires. The "shadow deposition" process employed here has been used and studied in the past [27] and is used successfully here to protect the imprinted sidewall from broadening during reactive-ion etching and in defining a smaller feature size in the final pattern. The 7-nm diameter Si features on the mold have been transformed into 22 and 25-nm features of Pt on alumina and silica, respectively. Despite the shadow deposition, there is still significant broadening in the features indicating that the broadening originates during the imprint process. It was found that the post-spin bake was not long enough to evaporate all of the solvent from the polymer. So upon heating up to the imprinting temperature, the remaining solvent evaporates and broadens the features [28]. This problem is currently being addressed. An AFM image of the 22-nm Pt nanowire array on an alumina substrate is pictured below in figure 3b and an SEM image of the same sample is shown in figure 3c. A 64-nm Pt nanowire array on silica was also prepared by NIL without the use of the shadow deposition process.

2.3. Characterization

The Pt nanoarrays were characterized by scanning electron microscopy (SEM), atomic force microscopy (AFM), and X-ray photoelectron spectroscopy (XPS). SEM images are taken with a JEOL JSM-6340F equipped with a cold field emission source operating between 3 kV and 20 kV with a probe current of 12 μA. All SEM images are acquired using an E–T combined backscatter and secondary electron detector at a working distance of 6 mm. Typical SEM images of the samples are shown in figures 1c, 2b, c, and 3c. AFM is used to determine the height and periodicity of the arrays. AFM images of the nanoparticle arrays are taken on a Park Scientific Instruments, M5 AFM. AFM images of the nanowire arrays are taken on a Molecular Imaging PicoSPM. Both AFM's use a feedback loop between a scan piezo and a position-sensitive photodiode array at a constant force to monitor the reflected laser light from the backside of the cantilever. Typical AFM images of the samples are shown in figures 1b and 3b. XPS spectra are taken to analyze the chemical composition of the surface after fabrication. Spectra are taken on a 15-kV, 40-Watt PHI 5400 ESCA/XPS system equipped with a Mg anode X-ray source. Samples are cleaned of any foreign particulates before being analyzed with a stream of nitrogen gas. The spectra are inspected for the Pt $4f_{7/2}$ and $4f_{5/2}$ peaks to verify that platinum had been deposited. As well, the spectra verify the presence of the characteristic Si and Al peaks for each of the oxide substrates.

2.4. Reaction apparatus

The reaction studies are carried out in an ultrahigh vacuum (UHV) chamber equipped with a high-pressure reaction cell. The general design of this type of chamber has been described elsewhere [29]. The outer chamber achieved a working pressure of 1×10^{-9} Torr between reactions. The chamber was evacuated by use of a turbomolecular pump (Balzers TPU 330), and an ion pump (Varian). All of the nanocatalyst arrays are cleaned by dosing with 1×10^{-6} Torr of NO_2 at 573 K for 20 min, followed by dosing the sample with 10 L of CO and flashing the temperature to 573 K to remove the remaining CO from the surface. This procedure has been established to be effective for cleaning supported Pt nanostructures and Pt(111) single crystals of their major surface impurities such as carbon and oxygen [30]. This cleaning procedure is used before the start of every experiment. The catalyst samples are mounted on a ceramic heater (Advanced ceramics, HT-01) with Ta clips. The temperature of the surface is measured with a 0.010-in. diameter chromel/alumel thermocouple wire. The thermocouple wire is clamped to the sample with a Ta clamp and an alumina spacer. The alumina spacer is used to avoid electrical contact between the heater and the thermocouple. Auger electron spectroscopy (AES) is used to monitor the surface cleanliness of the sample. All Auger spectra are taken using a Physical Electronics Industries, Inc. Auger system. As the Auger process itself can deposit carbon impurities on the surface of the sample, the sample is always cleaned after any Auger spectra are taken. A schematic of the UHV reaction system is shown in figure 4.

2.5. Reaction studies

Every sample is cleaned as described above before introducing reaction gases. Catalytic studies are carried out on all catalyst samples using 10 Torr C_2H_4, 100 Torr H_2, and 650 Torr Ne gas. For CO poisoning studies, 300 mTorr of CO is added to the manifold with the reaction gases. Gases are premixed in the gas manifold approximately 20 min before introduction to the catalyst and the reaction line. The gases are circulated through the reaction line with a Metal Bellows re-circulation pump. A HP Series II gas chromatograph equipped with a FID detector and a 50-m alumina capillary column (J & W Scientific) was used to separate and analyze products. The GC was part of the reaction loop and sampled the circulating reaction gases every 2.5 min using an automatic sampling valve. The H_2,

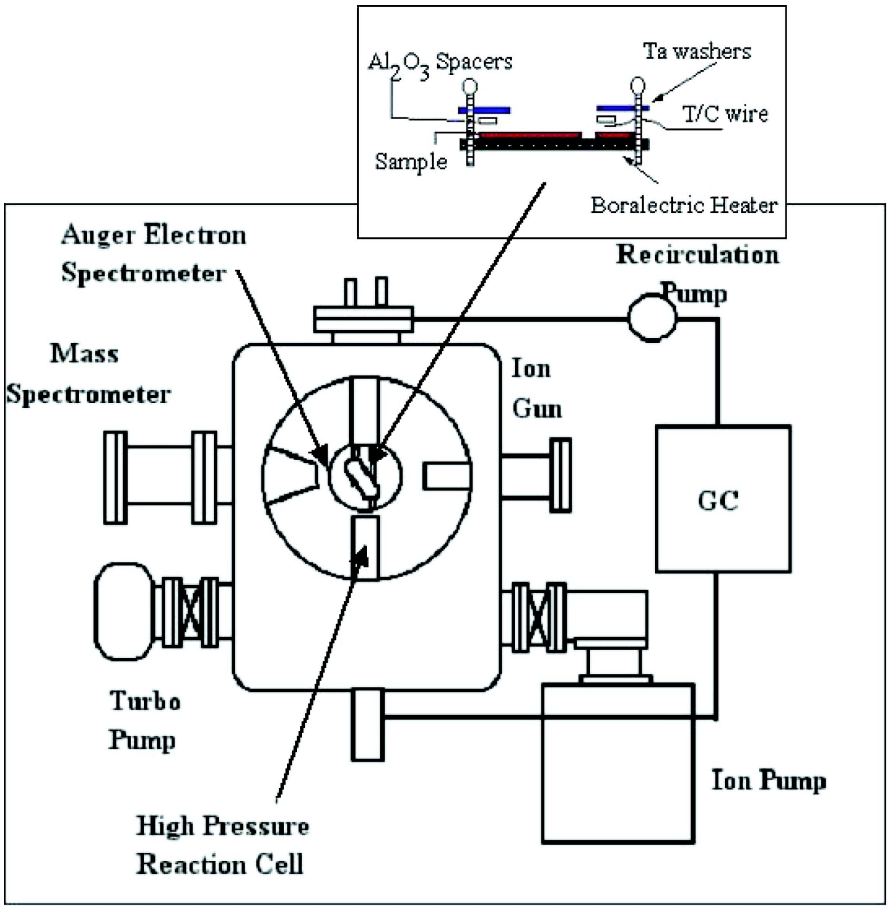

Figure 4. Schematic of UHV reaction system. Inset shows the sample mount used for reactions.

C_2H_4, Ne, and CO had gas purities of 99.99, 99.5, 99.999, and 99.3%, respectively.

3. Results

3.1. Nanoparticle samples on alumina and silica

SEM images show the diameter of the Pt particles on both alumina and silica to be 28 ± 2 nm and the periodicity to be 100 ± 1 nm. A representative SEM image of the fabricated Pt nanoparticles is shown in figure 1c. The area of the EBL arrays both on alumina and silica are 36 mm^2 equivalent to 3.6×10^9 Pt particles. AFM measurements verify the height of the nanoparticles to be 15 ± 1 nm as shown in figure 1b. The array pictured in figure 1 is that of Pt particles on an alumina substrate.

3.2. Nanowire samples on alumina and silica

SEM images of the nanowire arrays on silica and alumina show the nanowire diameters to be 64 ± 3 nm and 25 ± 2 nm on silica, and 22 ± 2 nm on alumina. SEM measurements also show the distance in the middle of the wire to be 600 ± 3 nm and between two different wires to be 1072 ± 4 nm for the 64-nm Pt wires, 1150 ± 3 nm for the 25-nm Pt wires, and 1156 ± 3 nm for the 22-nm Pt wires. AFM images of the nanowires, show them to have a height of 15 ± 1 nm (figure 3b) and confirm the width of the Pt features. AFM and SEM images in figure 3b and c, respectively are that of the 22-nm nanowires on an alumina substrate.

3.3. Reaction studies

The ethylene hydrogenation reaction studies over the various catalyst arrays were carried out in the 313–413 K temperature range without the presence of CO and in the 393–473 K temperature range with the presence of CO. This is a structure insensitive reaction on platinum catalysts, meaning that under most conditions the turnover rate will be the same for different platinum catalysts reacting under similar conditions. A summary of the measured activation energies and the turnover rates at 300 K is shown below in table 1 for all of the fabricated catalysts. A typical ethane accumulation curve is shown in figure 5. The accumulation curves yield the rate of reaction at different temperatures and using this information, Arrhenius plots are constructed to obtain the apparent activation energy of reaction. Due to the small metal surface area of the catalyst

Table 1
Summary of reaction studies

Catalyst sample	Unpoisoned E_a (kcal mol^{-1})	CO poisoned E_a (kcal mol^{-1})	Unpoisoned turnover frequency at 300 K (s^{-1})	Poisoned Turnover frequency at 300 K (s^{-1})
Pt (111) [31,32]	10.8 ± 0.1	20.2 ± 0.1	10	4.8×10^{-6}
28-nm Pt nanoparticles on alumina support	10.2 ± 0.2	11.4 ± 0.5	7.3	0.071
28-nm Pt nanoparticles on silica supportc	11.3 ± 0.1	15.6 ± 0.4	5.3	0.041
22-nm Pt nanowires on alumina support	13.6 ± 0.2	21.3 ± 0.2	14	5.0×10^{-5}
25-nm Pt nanowires on silica support	13.5 ± 0.1	22.2 ± 0.3	11	1.4×10^{-5}
64-nm Pt nanowires on silica support	13.0 ± 0.3	19.8 ± 0.3	9.1	7.9×10^{-5}

samples, ethane accumulation is slow at room temperature. Therefore, all reported turnover rates have been extrapolated from the Arrhenius plots to recover the turnover rates at 300 K. The reactions on the fabricated catalysts will be compared to the reaction studies on Pt(111) single crystal by Zaera *et al.* [31] and Hwang *et al.* [32] The single crystal data shows a turnover rate of 10 s^{-1} and an activation energy of 10.8 ± 0.1 kcal mol^{-1} with no CO poisoning. Upon CO poisoning, the turnover rate decreases sharply to 4.8×10^{-6} s^{-1} and there is a corresponding increase in the activation energy to 20.2 ± 0.1 kcal mol^{-1}. The turnover rate of for the Pt(111) single crystal was calculated using the empirical rate equation of Zaera *et al.* [31] The turnover rate for the CO poisoning of the single crystal was extrapolated from the Arrhenius plot in Ref. 32.

The Pt nanoparticle arrays, both on silica and alumina, show similar behavior for the unpoisoned ethylene hydrogenation studies. However, the CO-poisoned reaction studies have dramatically different behavior than the Pt(111) single crystal. Unpoisoned ethylene hydrogenation studies on the silica and alumina supported catalysts show apparent activation energies of 11.3 ± 0.1 kcal mol^{-1} and 10.2 ± 0.2 kcal mol^{-1} and turnover rates of 5.3 s^{-1} and 7.3 s^{-1}, respectively. As

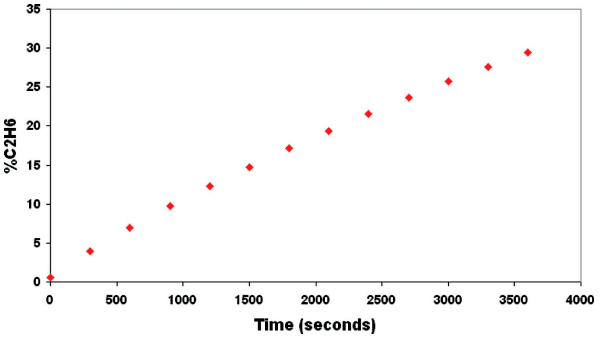

Figure 5. Typical ethane accumulation curve used to calculate turnover rates. This data was obtained at 353 K using a Pt nanoparticle catalyst on a silica support.

mentioned above, these numbers are similar to those seen for the Pt(111) single crystal. The activation energies are almost identical to that of Pt(111), and the turnover rates are close to the accepted value of ~10 s^{-1}. The CO poisoning studies show that the nanoparticle arrays have a lower energy of activation than seen with CO-poisoned Pt(111). The silica and alumina supported arrays show apparent activation energies of 15.6 ± 0.4 kcal mol^{-1} and 11.4 ± 0.5 kcal mol^{-1}, and turnover rates of 0.041 s^{-1} and 0.071 s^{-1}, respectively. The activation energies are significantly lower than that measured on CO-poisoned Pt(111), and the turnover rates are four orders of magnitude higher than that seen for the single crystal. The Arrhenius plots for these two samples are shown in figure 6a, b.

A size comparison was done for Pt nanowires on a silica support with nanowires of diameters 25 nm and 64 nm. Unpoisoned ethylene hydrogenation measured on these wire samples shows apparent activation energies of 13.5 ± 0.1 kcal mol^{-1} and 13.0 ± 0.3 kcal mol^{-1}, and turnover rates of 11 s^{-1} and 9.1 s^{-1}, respectively. The measured activation energies are a bit higher than that measured for the Pt(111) and Pt nanoparticles, but the turnover rates are around the accepted value of 10 s^{-1}. CO poisoning of the reaction measured on the 25-nm wires show an apparent activation energy of 22.2 ± 0.3 kcal mol^{-1} and a turnover rate of 1.4×10^{-5} s^{-1}. The 64-nm nanowire array show an apparent activation energy of 19.8 ± 0.3 kcal mol^{-1} and a turnover rate of 7.9×10^{-5} s^{-1} for the CO poisoning study. Both arrays have a 6 order of magnitude drop in the turnover rate upon CO poisoning whereas the Pt(111) shows a drop of seven orders of magnitude. The difference in wire diameter of the two arrays did not make a difference in their reactivities in comparison to each other. Both arrays have almost identical turnover rates and activation energies. Next, these reactions were studied on a sample of 22-nm diameter Pt nanowires on an alumina support. This sample was considered comparable in wire size to the 25-nm Pt nanowire sample on

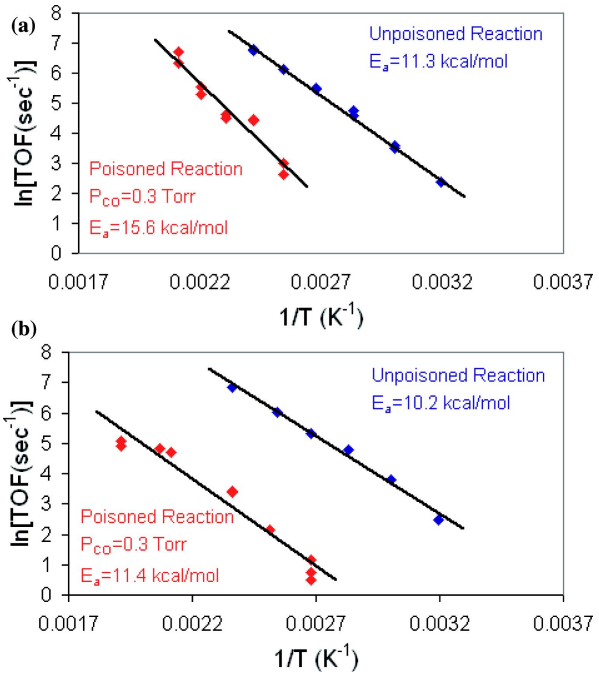

Figure 6. Arrhenius plots for ethylene hydrogenation reactions on Pt nanoparticle arrays supported on (a) silica and (b) alumina.

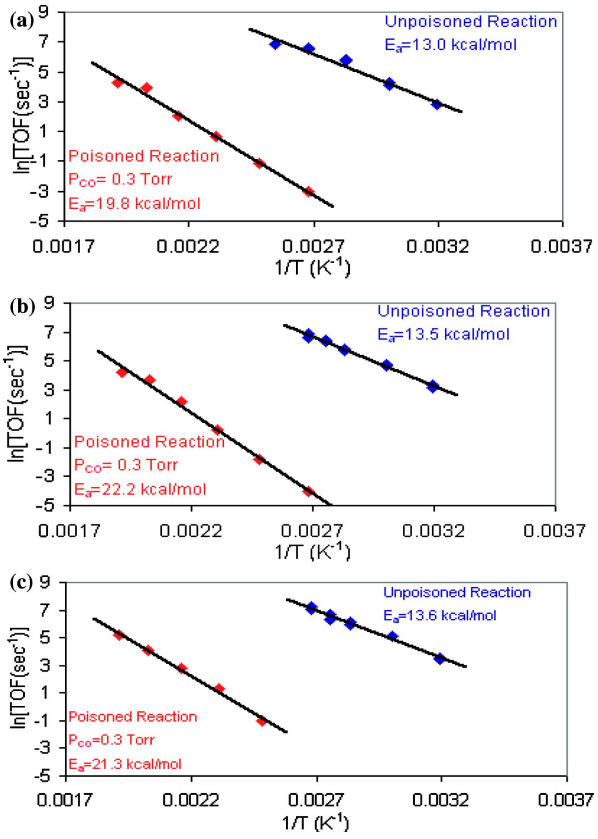

Figure 7. Arrhenius plots for ethylene hydrogenation reactions on Pt nanowires arrays. (a) 64-nm diameter Pt nanowires on silica support. (b) 25-nm diameter Pt nanowires on silica support. (c) 22-nm diameter Pt nanowires on alumina support.

silica. The 22-nm Pt nanowires on alumina show an unpoisoned activation energy of 13.6 ± 0.2 kcal mol^{-1} with a turnover rate of 14 s^{-1}. CO poisoning of the catalyst gives a measured activation energy of 21.3 ± 0.2 kcal mol^{-1} with a turnover rate of 5.0×10^{-5} s^{-1}. The apparent activation energies of the 22-nm and 25-nm samples are almost identical for both the unpoisoned and CO-poisoned reactions. The unpoisoned turnover rate on the alumina-supported nanowires, however, is higher than any of the other catalyst samples. The poisoned turnover rate on the alumina-supported nanowires drops 6 orders of magnitude as the silica-supported samples did, which again, gives a turnover rate that is about an order of magnitude higher than that of the Pt(111) after CO poisoning. The Arrhenius plots for the reaction studies conducted on these three nanowire samples is shown in figure 7a-c.

4. Discussion

Table 1 summarizes the turnover rates and activation energies for ethylene hydrogenation on the platinum nanoparticles and nanowires deposited on silica or alumina with and without CO poisoning. These results are also compared with similar data obtained on the (111) crystal face of platinum, which may be used as a reference state of a platinum catalyst without the presence of an oxide support. In order to calculate the turnover rates for each of the fabricated catalyst arrays, the metal surface area was calculated using geometrical considerations. For the nanoparticle samples, the nanoparticle geometry was considered to be that of a cylinder standing on an oxide support with a diameter of 28 nm and a height of 15 nm. For the nanowire samples, the nanowire wall geometry was considered to be that of a rectangle standing on an oxide support with a height of 15 nm, and the top of each wire was also considered to be rectangular. As well, the half circles on either end of the wires were considered and measured as cylindrical arcs standing on an oxide support. The platinum and oxide surface areas that result from these calculations are shown in table 2. Without the presence of oxide, the clean Pt(111) surface has a turnover rate of about 10 s^{-1} at 300 K and an activation energy of about 11 kcal mol^{-1}. The oxide-supported platinum nanoparticles and nanowires have very similar turnover rates with the exception of the alumina-supported nanowires, which have a 40% higher value. Also, the activation energies for the ethylene hydrogenation are about 2 kcal mol^{-1} higher (~13 kcal mol^{-1}) for the platinum nanowire systems than the activation energies for either the platinum single crystal or for the platinum nanoparticles. The reasons for these differences are yet to be determined and await vibrational spectroscopy studies using sum frequency generation, which may reveal

Table 2
Comparison of catalyst metal and oxide surface areas

Catalyst sample	Total Pt surface area (cm^2)	Oxide Surface Area (cm^2)	Ratio of oxide to metal surface area
28-nm Pt nanoparticles on alumina support	0.070 ± 0.006	0.34 ± 0.01	4.9 ± 0.4
28-nm Pt nanoparticles on silica support	0.070 ± 0.006	0.34 ± 0.01	4.9 ± 0.4
22-nm Pt nanowires on alumina support	0.066 ± 0.003	1.2 ± 0.1	18 ± 2
25-nm Pt nanowires on silica support	0.060 ± 0.003	1.0 ± 0.1	17 ± 2
64-nm Pt nanowires n silica support	0.10 ± 0.01	1.0 ± 0.1	9.8 ± 1

adsorbed surface species on these catalysts in addition to that of ethylidyne.

Major differences in catalytic behavior emerge, however, when the platinum catalysts are poisoned by adsorbed carbon monoxide. CO binds strongly to platinum and thus adsorbs preferentially to other gases in the reaction mixture like ethylene. Before a reaction can occur, a CO molecule must desorb from the metal surface. CO also restricts the mobility of the adsorbed reactant molecules, therefore lowering the probability of a reaction occurring. For Pt(111), CO poisoning of the reaction increases the activation energy to 20 kcal mol^{-1}, and decreases the turnover rate at 300 K by seven orders of magnitude, to approximately 10^{-6} s^{-1}. Similar results are obtained for the platinum nanowires. The activation energy for the reaction on the poisoned Pt-wire surface is around 20–22 kcal mol^{-1}. However, turnover rates are about an order of magnitude higher, $\sim 10^{-5}$ s^{-1} as compared to Pt(111). The CO-poisoned turnover frequencies for the nanowire arrays and Pt(111) are extremely low values and are extrapolated from actual data. Therefore, it is difficult to state clearly if the nanowires samples are displaying the same behavior as the Pt(111) or if there is some resistance to CO-poisoning.

Upon CO adsorption, the platinum nanoparticle arrays show dramatically different behavior than the Pt(111) single crystal and the platinum nanowires. The CO-poisoned activation energy for ethylene hydrogenation on alumina and silica is 11.4 kcal mol^{-1} and 15.6 kcal mol^{-1}, respectively. These are much lower than for either the Pt single crystal or the nanowire system. The turnover rates are in the range of $\sim 5 \times 10^{-2}$ s^{-1}, which is orders of magnitude greater than for the single crystal or for nanowire surfaces. It appears that on these platinum nanoparticle arrays deposited on the oxides (SiO_2 or Al_2O_3), there are reaction sites that do not deactivate for ethylene dehydrogenation in the presence of coadsorbed carbon monoxide. These sites may be at the oxide-metal interfaces. An attempt was made to correlate the Pt-oxide interface sites to the turnover seen during CO-poisoning of the reaction by calculating the turnover rates and considering them to be a consequence of either the total amount of Pt on the surface of the nanoparticle or of just the oxide-Pt interface sites on the surface. The interface sites were calculated geometrically by using the circumference of a Pt nanoparticle. The results of these calculations are shown in table 3. The unpoisoned turnover frequencies for the Pt nanoparticle samples on Al_2O_3 and SiO_2 are 7.3 s^{-1} and 5.3 s^{-1}, respectively. If the same amount of platinum is taken into consideration (i.e. the platinum surface area of the entire particle), then the CO-poisoned turnover frequencies for the Al_2O_3 and SiO_2 supported samples are 0.071 s^{-1} and 0.041 s^{-1}, respectively. However, if the interface sites are considered to be the only active sites for reaction during CO poisoning, and the turnover frequency is calculated from just these sites alone, then the Al_2O_3 and SiO_2 supported samples have turnover frequencies of 7.1 s^{-1} and 4.2 s^{-1}, respectively. These turnover frequencies are almost identical to those of the unpoisoned samples. While not conclusive, these results do lend credence to the idea of oxide-metal interface sites remaining active under poisoning conditions. Varying

Table 3
Comparison of turnover frequencies between the two EBL-fabricated catalyst samples

Catalyst Sample	Unpoisoned turnover frequency at 300 K (s^{-1})[a]	CO-poisoned turnover frequency at 300 K (s^{-1})[b]	CO-poisoned turnover frequency at 300 K (s^{-1})[c]
28-nm Pt nanoparticles on alumina support	7.3	0.071	7.1
28-nm Pt nanoparticles on silica support	5.3	0.041	4.2

[a] Unpoisoned turnover frequencies.
[b] CO-poisoned turnover frequencies calculated assuming all Pt surface sites are active.
[c] CO-poisoned turnover frequencies assuming only oxide-Pt interface sites are active. Pt surface sites and oxide-Pt interface sites were determined by geometrical considerations.

the EBL platinum particle size and determining if the CO-poisoned turnover frequency scales accordingly can perhaps elucidate this idea further.

These investigations of the catalytic behavior of platinum model catalysts of different structures using a single reaction such as ethylene hydrogenation point to the existence of active sites other than the platinum metal sites. These active sites may allow the continued catalytic activity for some supported platinum catalysts as compared to the rapid deactivation of platinum crystal surfaces or thin films during hydrocarbon conversion. More studies using other reactions and other oxide supports are in progress.

5. Conclusion

EBL, SRL, and NIL techniques can be used successfully to create model catalysts in the sub-100 nm size regime. These fabricated catalysts have proven to be viable model catalysts by use of ethylene hydrogenation as a probe reaction. EBL platinum nanoparticle samples have demonstrated the ability to resist poisoning by carbon monoxide, and a correlation has been made between the number of oxide-Pt interface sites and the CO-poisoned turnover frequency. Further studies using samples with various sizes as well as incorporation of spectroscopy into the study will help shed some light on the pertinent surface chemistry.

Acknowledgments

We would like to thank Dr Ji Zhu of Lam Research Corporation, Dr E.A. Anderson of Lawrence Berkeley National Laboratory, Professor J. Bokor, and Professor Y.K. Choi both of UC Berkeley EECS Department, for all of their contributions to this work. This work was supported by the Director, Office of Science, Office of Basic Energy Sciences, Chemical and Materials Sciences Divisions, of the US Department of Energy under Contract No. DE-AC03-76SF00098.

References

[1] M. Salmeron and G.A. Somorjai, J. Phys. Chem. 85 (1981) 3835.
[2] M. Salmeron and G.A. Somorjai, J. Phys. Chem. 86 (1982) 341.
[3] S.M. Davis and G.A. Somorjai, J. Phys. Chem. 87 (1983) 1545.
[4] X. Su, P.S. Cremer, Y.R. Shen and G.A. Somorjai, J. Am. Chem. Soc. 119 (1997) 3994.
[5] K.R. McCrea, J.S. Parker and G.A. Somorjai, J. Phys. Chem. B 106 (2002) 10854.
[6] J. Horiuti and M. Polanyi, Trans. Faraday Soc. 30 (1934) 1164.
[7] F. Zaera and G.A. Somorjai, J. Catal. 84 (1983) 375.
[8] F. Zaera and G.A. Somorjai, Langmuir 2 (1986) 686.
[9] F. Zaera and G.A. Somorjai, J. Phys. Chem. 89 (1985) 3211.
[10] D. Godbey, F. Zaera, R. Yeates and G.A. Somorjai, Surf. Sci. 167 (1986) 150.
[11] A.L. Backman and R.I. Masel, J. Vac. Sci. Technol. 6 (1988) 1137.
[12] A.L. Backman and R.I. Masel, J. Vac. Sci. Technol. 9 (1991) 3.
[13] P. Cremer, C. Stanners, J.W. Niemantsverdriet, Y.R. Shen and G.A. Somorjai, Surf. Sci. 328 (1995) 111.
[14] T. Ohtani, J. Kubota, J.N. Kondo, C. Hirose and K. Domen, J. Phys. Chem. B 103 (1999) 4562.
[15] R. Deng, E. Herceg and M. Trenary, Surf. Sci. 560 (2004) L195.
[16] D.C. Tang, K.S. Hwang, M. Salmeron and G.A. Somorjai, J. Phys. Chem. B 108 (2004) 13300.
[17] A.S. Eppler, J. Zhu, E.A. Anderson and G.A. Somorjai, Top. Catal. 13 (2000) 33.
[18] J. Zhu and G.A. Somorjai, Nano. Lett. 1 (2001) 8.
[19] C.H. Ting and K.L. Liauw, J. Vac. Sci. Technol. B 1 (1983) 1225.
[20] S.A. Rishton and D.P. Kern, J. Vac. Sci. Technol. B 5 (1987) 135.
[21] M.T. Bohr, Appl. Surf. Sci. 101 (1996) 534.
[22] Y.K. Choi, J. Zhu, J. Grunes, J. Bokor and G.A. Somorjai, J. Phys. Chem. B 107 (2003) 3340.
[23] Y.K. Choi, J.S. Lee, J. Zhu, G.A. Somorjai and J. Bokor, J. Vac. Sci. Tech. B 21 (2003) 2951.
[24] S.Y. Chou, P.R. Krauss and P.J. Renstrom, Appl. Phys. Lett. 67 (1995) 3114.
[25] S.Y. Chou, P.R. Krauss and P.J. Renstrom, Science 272 (1996) 85.
[26] S.Y. Chou, P.R. Krauss, W. Zhang, L.J. Guo and L. Zhuang, J. Vac. Sci. Technol. B 15 (1997) 2897.
[27] L.F. Johnson, K.A. Ingersoll and G.W. Kammlott, Appl. Phys. Lett. 34 (1979) 578.
[28] C. Gourgon, J.H. Tortai, F. Lazzarino, C. Perret, G. Micouin, O. Joubert and S. Landis, J. Vac. Sci. Technol. B 22 (2004) 602.
[29] E. Segal, R.J. Madon and M.J. Boudart, Catal. 52 (1978) 45.
[30] J. Grunes, J. Zhu, E.A. Anderson and G.A. Somorjai, J. Phys. Chem. B 106 (2002) 11463.
[31] F. Zaera and G.A. Somorjai, J. Am. Chem. Soc. 106 (1984) 2288.
[32] K.S. Hwang, M. Yang, J. Zhu, J. Grunes and G.A. Somorjai, J. Mol. Catal. A 204–205 (2003) 499.